ORIGINAL SCIENTIFIC PAPER

CROATICA CHEMICA ACTA

Croat. Chem. Acta **2025**, *98*(1), 37–51
Published online: May 18, 2025
DOI: 10.5562/cca4096

HKD 1926

Efficient Removal of Hexavalent Chromium with Novel Agro-Waste Biochar

Tayyab Ashfaq-Butt

Department of Civil Engineering, College of Engineering, University of Hail, Ha'il 55425, Saudi Arabia
* Corresponding author's e-mail address: ta.butt@uoh.edu.sa

RECEIVED: April 12, 2024 ⋆ REVISED: March 14, 2025 ⋆ ACCEPTED: March 14, 2025

Abstract: The suitability of beechwood chip biochar(BC1) and garden green waste biochar (BC2) for Cr(VI) removal was explored in this study. Green waste biochar (BC2) was found to be the most effective for Cr(VI) removal (84.6 %) at room temperature at an adsorbent dose of 10 g L^{-1} at an optimum pH of 5. The Freundlich isotherm model exhibited the best fit, followed closely by the Langmuir model, suggesting a heterogeneous adsorption process with a potential contribution from monolayer adsorption, as supported by nine error functions. Adsorption kinetics was best explained by pseudo nth-order model (PNO). Gibbs free energy (ΔG) was found to vary between –24.19 to –29.48 (BC1) and –24.18 to –28.39 483 kJ mol^{-1}(BC2), indicating a spontaneous reaction. Enthalpy (ΔH) was 74.483 kJ $mol^{-1}$for BC1 and 59.51 483 kJ $mol^{-1}$for BC2, which indicates chemisorption in the current study.

Keywords: beechwood, garden green waste, chromium, error function analysis, PNO model.

INTRODUCTION

WATER contamination by heavy metals is a major environmental global concern with chromium being one of the most hazardous contaminants Chromium pollution is a significant environmental threat, severely impacting our environment and natural resources, especially water and soil.[1] Cr has been ranked as Group1 carcinogen by International Agency for Research on Cancer.[2] Anthropogenic sources of Cr are from industrial sources, particularly from industrial processing and manufacturing of chemicals, minerals, steel, metal plating, leather tanning, textile dyeing, electroplating, and cement production, metallurgical and other works.[3] Additionally, improper disposal of chromium-containing waste and runoff from agricultural practices using chromium-based pesticides contributes significantly to chromium pollution in water and soil. Chromium in form of hexavalent Cr(VI) is considered as 100 time more toxic as compare to Cr (III) because of more availability mostly when pH of solution or soil is more than 2.[4] Cr(VI) levels in contaminated environment can vary greatly, ranging from negligible amounts to concentrations above 5 mg L^{-1} in industrial effluents, much above the World Health Organization's (WHO) allowed limit of 0.05 mg L^{-1} for drinking water.[5] Several studies have shown that chromium is a toxic element that negatively affects plant metabolic activities, hampering crop growth and yield and reducing vegetable and grain quality. The hexavalent chromium has carcinogenic, teratogenic, and mutagenic properties, so it has been identified as a priority pollutant.[6] Thus, it must be monitored in water, soil, and crop production system. Various useful and practical remediation technologies including ion exchange, membrane filtration, electrochemical methods, and advanced oxidation processes have been emerging in regulating chromium in water, soil, and other resources.[7] While effective, these methods often involve certain limitation such as high operational costs, energy and time consumption. A sustainable remediation approach must be adopted to balance the environment and nature. Therefore, sorption, particularly utilizing low-cost and sustainable adsorbent, has arisen as alternative approach for Cr(VI) removal due to its simplicity, cost-effectiveness, and environmental compatibility. Several studies in literature have evaluated biochar for the removal of various toxic metals, including arsenic, lead, cadmium, and mercury.[8] Its application for chromium removal has also been reported, demonstrating significant adsorption capacity under optimized conditions. Due to

minimal requirement for pre-treatment, low cost of production and large-scale availability, biochar offers immense potential for Chromium remediation.[9] Furthermore, biochar has been utilized in agriculture, soil remediation, carbon sequestration, and wastewater treatment, emphasizing its multifunctionality and environmental benefits.

Four mechanisms dominating heavy metals removal from water by biochar have been proposed which are as follows (i) electrostatic attraction between heavy metals and biochar surface; (ii) ion exchange between heavy metals and alkali or alkaline earth metals or protons on biochar surface; (iii) complexation with electron-rich domain or surface functional groups; (iv) co-precipitation to form insoluble compounds.[10] It has found that the Cr (VI) can be removed by pristine biochar in an acid condition.[11,12] At lower pH values, oxygen functional groups present on biochar undergo protonation and the protonated form of biochar interact the Cr(VI) through electrostatic mode.[10] Also, it has been found that with pH less than $pH_{PZ^{\circ}C}$, the electropositive surface functional groups derived from protonation enhance the electrostatic attraction to electronegative Cr species.[13] In addition, the positively charged surface reduces the competitive adsorption of OH^- anions and supplies protons for the reduction of Cr (VI).[14]

Thus, biochar fabricated from wood, algae, and switchgrass, with acidic pH levels of 3 to 5.8, have been found to be more suitable for Cr(VI) adsorption.[15] Also it has been found that the feedstock source with a low lignin content produced abundant functional groups on biochar, and higher pyrolysis temperature improved the surface area of biochar, making it more conducive to the removal of hexavalent chromium which in most cases was sorption and reduction of Cr(VI) by the biochar.[16]

Therefore, the influence of biomass composition and pyrolysis temperature on the performance of biochar still needs more exploration. In the present study, the characteristic feedstock with different biomass compositions were selected for biochar production. The objectives of this study were as follows:

- To compare the effect of the two types of biochars, i.e., Beech wood chip(BC1) and green garden waste (BC2) for Cr(VI) removal from contaminated water
- To gain a deeper understanding of the process of Cr(VI) sorption by biochar through isotherm, kinetic and thermodynamic studies.

MATERIALS AND METHODS

Chemical Reagents

All the chemicals used in the study were of analytical grade. All the glassware was washed with 0.1 N HNO_3. A chromium(VI) stock solution of 1000 mg L^{-1} was prepared by adding 14.3 g of $K_2Cr_2O_7$ to 500 mL of distilled water in a volumetric flask.

Biochar Preparation and Characterization

The biochars were prepared from two different feedstocks .Beech wood chips (BC1) and garden green waste (BC2) in a slow pyrolysis process at a temperature of 450–500 °C. The residence time in biochar formation was approximately 120–130 min. Nitrogen was used as an inert gas to maintain oxygen-depleted conditions. The biochars were ground to a size of < 1.5 mm. The biochars were pretreated with deionized water to eliminate the presence of any ash impurities. The dried biochars were then stored in an airtight desiccator prior to use. Some basic physicochemical properties of biochars, i.e. specific surface area, pore size, % ash, pH, electrical conductivity (EC) and cation exchange capacity (CEC) were determined according to Kloss et al.,[9] and the results are presented in Table 1. The physicochemical properties of the two types of biochars used in this study are given below.

Chromium Adsorption Experiments

All adsorption experiments were conducted in triplicates to ensure reproducibility and accuracy of results. A fixed volume of 50 mL Cr(VI) solution was used in 250 mL Erlenmeyer flasks with the required dose of biochar (BC). Kinetic experiments were first conducted at 25 °C to determine the contact time needed to reach sorption equilibrium, varying the contact time from 0 to 1440 minutes with initial Cr(VI) concentrations of 10 mg L^{-1}, using 2.5 g L^{-1} of BC at pH 5. Once equilibrium time was established, equilibrium sorption experiments were performed to investigate the effects of biochar dose and pH. The effect of biochar dose was examined by varying the adsorbent dose at 2.5, 5, 7.5, and 10 g L^{-1} while maintaining a fixed initial Cr(VI)

Table 1. Physicochemical properties of BC1 & BC2.

Parameters	Beech Wood Chip (BC1)	Garden Green Waste(BC2)
pH (H_2O)	8.78	9.03
pH (KCl)	8.46	8.77
EC (mS cm^{-1})	0.54	1.67
Ash content (%)	15.20	19.3
Density (kg m^{-3})	0.36	0.34
CEC (mmol / 100 mL)	9.83	12.85
SA (m^2 g^{-1})	27.24	31.54
C (%)	80.30	79.78
H (%)	1.60	1.59
N (%)	0.40	0.65

concentration of 10 mg L^{-1} at pH 5. Similarly, the effect of pH was analyzed by adjusting the initial solution pH to 5.0, 6.0, 7.0, and 8.0 ± 0.05 using 1 M HNO_3 or 1 M NaOH, keeping the initial Cr(VI) concentration at 10 mg L^{-1} and a biochar dose of 2.5 g L^{-1}. For all experiments, samples were shaken mechanically at a constant speed of 180 rpm for the required contact time. After shaking, biochar was separated by centrifugation at 5000 rpm for 5 minutes, and the solutions were filtered through a 0.22-µm filter. The absorbance of the filtered solution was measured at a specific wavelength of 355 nm. The isotherm and kinetic models used in the study are listed in Table 2.

Assessment of Cr by Atomic Absorption Spectroscopy

The Cr concentration in the water samples was determined by a Fast Sequential Atomic Absorption Spectrometer (wavelength 428.9nm at slit width 0.5 nm in acetylene fuel with air as support medium) (Varian FS-AA-240; Software version 5.01 Australia 1997–2003). Standards, made by diluting spectral pure grade chromium solution in 1:1 HCl at a concentration range of 1–100 mg L^{-1} were run before metal analysis. The absorbance of the metal was then analyzed by a spectrometer.[10]

Table 2. Isotherm and kinetic models used in the present study.

Model	Equation	Parameters
Isotherm models		
Langmuir[11]	$q_e = \frac{K_{ads} Q_{max} C_e}{1 + K_{ads} C_e}$ (1)	q_e (mg g^{-1}) - equilibrium adsorption capacity K_{ads} (L mg^{-1}) - Langmuir constant related to free energy of adsorption Q_{max}(mg g^{-1}) - maximum adsorbent capacity R_L separation factor C_0 (mg L^{-1}) - initial adsorbate concentration in solution C_e (mg L^{-1}) - equilibrium adsorbate concentration in solution
	$R_L = \frac{1}{1 + K_{ads} C_0'}$ (2)	
Freundlich[12]	$q_e = \frac{x}{m} = K_f C_e^{\,n}$ (3)	K_f (mg g^{-1}) (L g^{-1})^n - freundlich constant n - heterogeneity factor
BET[13]	$q_e = \frac{q_s C_{BET} C_e}{(C_S - C_e)\left[1 + (C_{BET} - 1)\frac{C_e}{C_S}\right]}$ (4)	C_{BET} - BET constant related to the energy of surface interaction (L mg^{-1}) C_s - adsorbate monolayer saturation concentration (mg L^{-1}) q_s - theoretical monolayer isotherm saturation capacity(mg g^{-1})
Pseudo 1st order[14]	$q_t = q_e(1 - e^{-k_1 t})$ (5)	q_t (mg g^{-1}) - amount of adsorbates adsorbed at time t k_1 (min^{-1}) - pseudo 1st order rate constant
Kinetic models (reaction models)		
Pseudo 2nd order[15]	$q_e = \frac{q_e^2 k_2 t}{1 + k_2 q_e t}$ (6)	k_2 (g mg^{-1} min^{-1}) - pseudo 2nd order rate constant h (mg g^{-1}.min^{-1}) - initial adsorption rate
	$h = k_2 q e^2$ (7)	
Ritchie's second order (RSO)[16]	$q_t = \frac{\alpha q_\alpha t}{1 + \alpha t}$ (8)	q_α - equilibrium adsorption capacity at infinite time (mg g^{-1}) α - RSO rate constant (min^{-1})
Pseudo n^{th} order (PNO)[17]	$q_t = q_e\left[1 - \frac{1}{\left[1 + (n-1)q_e^{n-1} k_n t\right]^{\frac{1}{n-1}}}\right]$ (9)	q_e - equilibrium adsorption capacity at infinite time (mg·g^{-1}) k_n - rate constant (min^{-1}) (mg g^{-1}) $^{(1-n)}$ n - order of equation
Kinetic models (Diffusion models)		
Weber Morris Intra-particle diffusion[18]	$q_t = k_i t^{1/2} + C_{ip}$ (10)	k_{ip} (mg g^{-1} $min^{-1/2}$) - intraparticle diffusion rate constant C_{ip} (mg g^{-1}) - boundary layer effect D_i (mm^2 min^{-1}) - liquid film effective diffusion coefficient d_p (mm) - diameter of adsorbent particle
	$k_{ip} = \frac{3q_e}{d_p}\sqrt{\frac{D_i}{\pi}}$ (11)	
Boyd's internal diffusion model[19]	$q_t = q_e\left[1 - \frac{6}{\pi^2} e^{-Bt}\right]$ (12)	B (/min^{-1}) - rate Coefficient for effective diffusion process D_i (mm^2 min^{-1}) - liquid film effective diffusion coefficient r (mm) - radius of adsorbent particle
	$B = \frac{\pi^2 D_i}{r^2}$ (13)	

Thermodynamic Studies

Thermodynamic studies are indispensable for predicting adsorption mechanisms (e.g., physical and chemical). Thermodynamic studies were conducted, and the thermal nature of the adsorption reactions was verified using the Gibbs equation.

$$\Delta G = \Delta H - T\Delta S \tag{14}$$

Thermodynamic parameters include the changes in Gibbs free energy (ΔG), enthalpy (ΔH) and entropy (ΔS) of the adsorption system. These parameters are the actual indicator to understand the thermodynamic state of the adsorbents during Cr(VI) adsorption. ΔG indicates that whether the reaction is spontaneous or nonspontaneous, ΔH determines the exothermic and endothermic nature, and ΔS reveals the high or lower degree of disorder at the solid–liquid interface during the chemical reaction. These parameters were determined by the following [Eq. (14–18)].

Thermodynamic parameters can be computed using the equation

$$\Delta G^{\circ} = -RT\ln(K_c) \tag{15}$$

where R is universal gas constant (8.314 J mol^{-1} K^{-1}), T is absolute temperature in Kelvin, and K_C is equilibrium constant.

The value of K_C can be estimated according to the method used by Zhou et al.,[20] who recommended that K_C could be obtained as a dimensionless parameter by using [Eq 20]:

$$K_c = M_w \cdot 55.5 \cdot 1000 \cdot K_L \tag{16}$$

where K_L is Langmuir constant L mg^{-1}, M_w is molecular weight of the adsorbate (g mol^{-1}), where the factor 55.5 is the number of moles of pure water per liter. Hence, substituting

$$\Delta G^{\circ} = -RT\ln(M_w \cdot 55.5 \cdot 1000 \cdot K_L) \tag{17}$$

The Gibbs energy change ($\Delta G°$) is directly calculated from [Eq. (17)] whereas the enthalpy change ($\Delta H°$) and entropy change ($\Delta S°$) are determined using nonlinear optimization of a plot of ln K_C versus 1 / T and then using the Van't Hoff equation, [Eq. (18)].

$$\Delta G^{\circ} = \left(\frac{\Delta H^{\circ}}{r} \cdot \frac{1}{T}\right) + \frac{\Delta S^{\circ}}{R} \tag{18}$$

Statistical Analysis

Experimentally obtained data were used for nonlinear regression analysis of various equilibrium and kinetic models. Various isotherm and kinetic models were checked using Microsoft Excel (Microsoft Office 2016, USA). The nonlinear least square technique via SOLVER based on the generalized reduced gradient (GRG) method of iteration available in Microsoft Excel was used to fit the experimental data to the selected models.

Error Functions

It is essential to determine the error functions to validate the goodness of fit for nonlinear isotherm models. To accomplish this task, the nonlinear isotherm data were computed to different error functions to obtain a holistic view of the optimum parameters and prediction of isotherms. The error distribution between the experimental and model-predicted values of adsorption capacities was minimized by reducing therespective error functions using solver add-in Microsoft® Excel 2013, and no constraints were applied during this minimization technique and optimization of model constants.

The studied error functions ([Eq. (19–27)] are as given below. The details of the studied error functions is given in literature.[21–26]

Coefficient of determination (R^2)

$$R^2 = \frac{\Sigma(q_{t_{cal}} - \overline{q}_{t_{exp}})^2}{\Sigma(q_{t_{cal}} - \overline{q}_{t_{exp}})^2 + \Sigma(q_{t_{cal}} - q_{t_{exp}})^2} \tag{19}$$

Nonlinear chi-square test (χ^2)

$$\chi^2 = \sum_{i=1}^{n} \frac{(q_{e_{exp}} - q_{e_{cal}})^2}{q_{e_{cal}}} \tag{20}$$

Average relative error (ARE)

$$\text{ARE} = \frac{100}{n} \sum_{i=1}^{n} \frac{(q_{t_{exp}} - q_{t_{cal}})^2}{q_{t_{cal}}} \tag{21}$$

Normalized standard deviation (NSD)

$$\text{NSD} = 100\sqrt{\frac{1}{n-1}\sum_{i=1}^{n}\left(\frac{q_{e_{exp}} - q_{e_{cal}}}{q_{e_{exp}}}\right)^2} \tag{22}$$

Marquardt's percent standard deviation (MPSD)

$$\text{MPSD} = 100\sqrt{\frac{1}{n-p}\sum_{i=1}^{n}\left(\frac{q_{e_{exp}} - q_{e_{cal}}}{q_{e_{exp}}}\right)^2} \tag{23}$$

Sum of absolute error (EABS)

$$\text{EABS} = \sum_{i=1}^{n} \left| q_{e_{exp}} - q_{e_{cal}} \right| \tag{24}$$

Hybrid functional error (HYBRID)

$$\text{HYBRID} = \frac{100}{n-p}\sum_{i=1}^{n}\frac{(q_{e_{exp}} - q_{e_{cal}})^2}{q_{e_{exp}}} \quad (25)$$

Sum of square of the error (ERRSQ)

$$\text{ERRSQ} = \sum_{i=1}^{n}(q_{e_{exp}} - q_{e_{cal}})^2 \quad (26)$$

Adjusted

$$R^2 = R^2_{\text{Adj}} = 1 - (1 - R^2)\frac{n-1}{n-p} \quad (27)$$

The parameters were optimized based on the sum of square errors(ERRSQ), and eight other error functions were checked for the optimum solution.

RESULTS AND DISCUSSION

Batch Adsorption Studies

The Cr adsorption capacities of biochars were studied over a contact time range of 0–1440 min, as shown in Fig.1(a). The BC2 biochar showed a higher adsorption capacity (9.49 mg g^{-1}) than the BC1 biochar (8.12 mg g^{-1}). Rapid Cr(VI) adsorpti on (12.7–16 %) occurred in 30–50 min due to the availability of more active sites on the adsorbents. This was followed by slow adsorption within 20–23 h. The equilibrium time was marked as 24 h for biochar. This has also been observed in a previous study.[8]

The pH varied from 5 to 8. The results of this experiment showed that a maximum Cr (VI) removal of 4.328 mg g^{-1} (BC1) and 5.13 mg g^{-1} (BC2) was observed at pH 5 with a 2.5 g L^{-1} adsorbent dose at an initial concentration of 10 mg L^{-1} (Figure 1 b). This decreased by increasing pH to 1.204 mg g^{-1} (BC1) and 2.672 mg g^{-1} (BC2) at pH 8. This has also been observed in previous studies where a decrease in pH from pH 5 to 2 has caused an increase in adsorption capacity.[3,4,27] At lower pH values, oxygen functional groups present on biochar undergo protonation, and the protonated form of biochar interacts with Cr (VI) through electrostatic mode.[4] Since the pH of both biochars was alkaline (8.78 BC1 & 9.08 BC2); hence, with pH less than pH_{Pzc}, the electropositive surface functional groups derived from protonation enhance the electrostatic attraction to electronegative Cr species.[5] In addition, the positively charged surface reduces the competitive adsorption of OH^- anions and supplies protons for the reduction of Cr(VI).[6] The highest metal removal rates of 78.1 % (BC1) and 84.6 % (BC2) were observed at pH 5 and an adsorbent dose of 10 g L^{-1}. The percent removal of metal decreased with increasing pH but increased with increasing adsorbent dose. The lowest Cr(VI) % removal from aqueous solution was observed at pH 8.

The increase in temperature (293–308 K) displayed an overall increase in the adsorption capacity (Fig. 1(c)(d)) from 7.2 to 9.8 % for BC1 and 8 to 10.8 mg g^{-1} for BC2 with an increase in the initial concentration from 1–80 mg L^{-1}. This result reflects the endothermic nature of the biochar adsorbent during the Cr 9-adsorption reaction. Previously, some researchers have demonstrated a constantly promoting effect of rising temperature on Cr(VI)removal efficiency (10 to 45 °C).[28–30] The enhancement in adsorption with arise in temperature from 20 to 35 °C can occur either due to the increase in the number of adhering sites on biochar, which are easily accessible for adsorption, or it may be due to the reduction in boundary layer thickness surrounding the biosorbent surface, which diminishes the mass transfer resistance to Cr(VI).[31] This increase in Cr(VI) adsorption with increasing temperature can also be related to the swelling of the pores of the biochars, which can accommodate more Cr(VI).[4]

The respective Cr(VI) adsorption capacities of biochar decreased, i.e., 1.352–0.781 mg g^{-1} (BC1) and 1.46–0.846 mg g^{-1} (BC2) with increasing adsorbent dose (Fig. 1(e)) because the adsorption capacity of the adsorbent is not fully utilized at a high adsorbent dose in comparison to a lower adsorbent dose. This might be due to the aggregation of the adsorbent due to increasing adsorbent dose, and this high adsorption density may decrease the available adsorption sites. However, the percentage removal of Cr(VI) increased from 33.8–78.1 % (BC1) and 36.5–84.6 % (BC2), contrary to the adsorption capacity obtained by increasing the adsorbent dose. This is because of the increasing number of grams of adsorbents per liter of adsorbate participating in removal, despite reduction per gram adsorption capacity. With a higher adsorbent dosage, biochar showed superior adsorption efficiency and lower Cr adsorption capacity.[30,32]

The increase in the initial concentration from 1 to 100 mg L^{-1} exhibited an increase in Cr(VI) adsorption capacities for biochar from 0.293 to 8.12 mg g^{-1} (BC1) and 0.333 to 9.49 mg g^{-1} (BC2) (Fig. 1(e)). This is because of the high mass transfer driving force, and this gradient is responsible for the larger number of Cr(VI) transfers towards the limited adsorbent surface. This causes an increase in the adsorption capacity with increasing initial Cr(VI) concentration. However, at higher Cr(VI) concentrations, the percentage removal decreased because of more residual Cr(VI) in solution.[33] The comparison table of BC1 and BC2 for different parameters have been given in supplementary information (Table S1 & S2).

Figure 2 illustrates the adsorption equilibrium data of Cr(VI) onto BC1 (a) and BC2 (b), with Langmuir, Freundlich, and BET isotherm models. The plots depict the relationship between adsorbate concentration C_e and

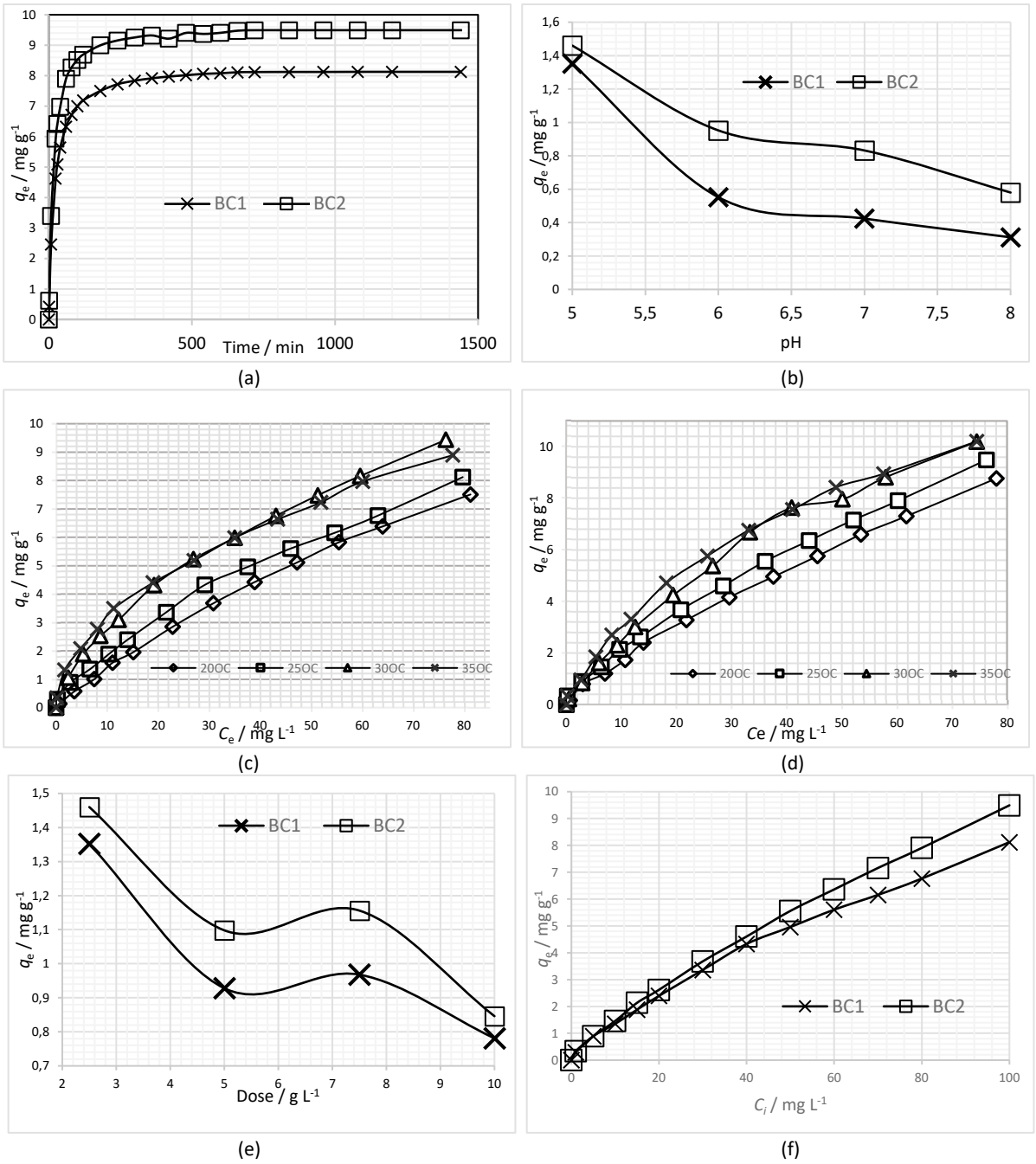

Figure 1. Effect of (a) contact time, (b) pH, (c) temperature for BC1, (d) temperature for BC2, (e) variable dose and (f) initial Cr(IV) concentration on biochar adsorption capacities.

adsorption capacity q_e at equilibrium, providing a comparison of how each model represents the experimental data. The equilibrium experiments for isotherm modeling were conducted by varying initial Cr(VI) concentrations at a room temperature. This figure helps to examine the feasibility of these models in illustrating the adsorption behavior of BC1 and BC2 adsorbent.

Application of Adsorption Isotherm Models

Various isotherm models were tested using nonlinear analysis to uncover the adsorption mechanism and the best fitting of the adsorption isotherm model can be judged based on nine error functions. Detailed statistical error analysis is provided in the Supplementary information in Table S3 and

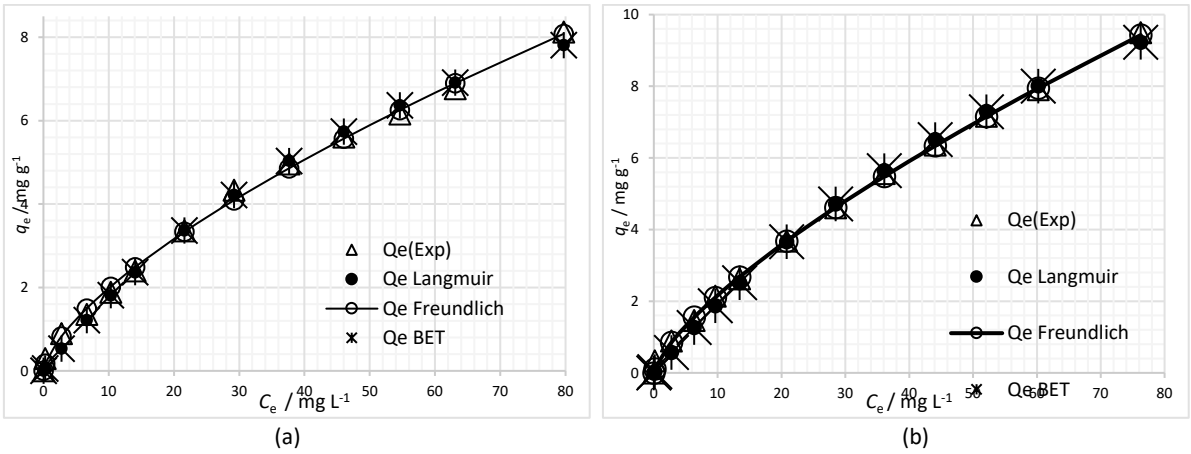

Figure 2. Cr(VI) adsorption data fit of (a) BC1 and (b)BC2 to the Langmuir, Freundlich, and BET isotherm models.

S4. The overall results obtained from the Langmuir, Freundlich and BET are summarized in Tables 3 & 4. For BC1, the maximum adsorption capacity, q_{max}, was calculated as 15.35 mg g^{-1} of Cr(VI), and K_L was calculated as 0.013 L mg^{-1}. The R_L value was found to vary from 0.987 to 0.435, reflecting a favorable adsorption process at 298.15 K. The decreasing value of R_L shows that the interaction between Cr(VI) molecules and the adsorbent increases as the concentration increases. The q_{max} for BC1 decreases with increasing temperature from 20.520 to 11.547 mg g^{-1}, while K_L increases from 0.0070 to 0.0344 L mg^{-1} with an increase in temperature from 20 °C to 35 °C.

For BC2 (Table 4), q_{max} was calculated as 21.5 mg g^{-1} of Cr(VI), and K_L was calculated as 0.00985 L mg^{-1}. The R_L value was found to vary from 0.99 to 0.5, reflecting a favorable adsorption process across the studied temperature range. The decreasing value of R_L shows that the interaction between Cr(VI) and the adsorbent increases as the concentration increases.[34] The q_{max} for BC2 decreased with an increasing temperature from 24.261 to 16.032 mg g^{-1}, while K_L increased from 0.0070 to 0.0225 L mg^{-1} with an increase in temperature from 20 °C to 35 °C. In both cases, the correlation coefficient for BC1(R^2 = 0.996) and BC2 (R^2 = 0.998) remained high, and ERRSQ (0.414 for BC1 and 0.454 for BC2) was intermediate, which indicates that this model is applicable in the current study.

In the Freundlich model, K_F for BC1 increases with increasing temperature from 0.244 to 1.021 mg g^{-1} (mg L^{-1})^n, while n increases from 1.274 to 1.957 with increasing temperature from 20 °C to 35 °C. The K_F for BC2 increases with increasing temperature from 0.293 to 0.781 mg g^{-1} (mg L^{-1})^n while n increases from 1.281 to 1.653 with increasing temperature from 20 °C to 35 °C. Additionally, it was notable that the value of n^{-1} varies from 0.785 to 0.51 for BC1 and 0.781 to 0.605 for BC2 by increasing the temperature from 20 to 35 °C, which indicates chemisorption as the dominant adsorptive force.[35] The error functions for the Freundlich model, such as ERRSQ,

Table 3. Isotherm models for Cr(VI) adsorption on BC1.

Isotherm Models	Parameters	20 °C	25 °C	30 °C	35 °C
Langmuir	q_m (mg g^{-1})	20.520	15.353	14.525	11.547
	K_L (L mg^{-1})	0.007	0.013	0.022	0.034
	R_L	0.99–0.585	0.987–0.435	0.979–0.32	0.979–0.32
	R^2	0.999776	0.996350	0.995525	0.988737
Freundlich	K_F(mg g^{-1}) / (mg L^{-1})^n	0.244	0.415	0.709	1.021
	n	1.274	1.474	1.671	1.957
	R^2	0.998440	0.998037	0.999309	0.999431
BET	Q_S (mg g^{-1})	19.673	14.933	14.237	11.364
	C_{BET} (L mg^{-1})	67.351	121.690	201.108	319.583
	C_S	9093.905	9093.001	9092.918	9089.708
	R^2	0.999777	0.996395	0.995618	0.988921

were lowest for BC1(0.166) and BC2 (0.072), while the R^2 values were highest for BC1 (0.998) and BC2 (0.999). As is clear from Figure 3, the error functions had the lowest value for this model; hence, this model provides the best fit to the current study. Based on the change in the n value with temperature, the BC1 surface is more heterogeneous than BC2.

As is clear from Tables 3 & 4, the correlation coefficient for both BC1 (R^2 = 0.999–0.989) and BC2 (R^2 = 0.999–0.998) for the BET model is high; however, the error function for this model has the highest value in both cases, indicating that the experimental data is not correlated with the BET model. This indicates that multilayer adsorption is not present in this case. This also indicates that in the current study, single-layer adsorption is present, which can be related to chemisorption.[36,37] Based on error functions (Table S3), isotherm fitting in terms of best to least is as follows: Freundlich > Langmuir > BET. Based on the isotherm analysis, the adsorption on both biochar is a single-layer heterogeneous adsorption.

Kinetics of Cr(VI) Adsorption on Biochar

The possible mechanisms of Cr(VI) transport towards the adsorbent surface include film diffusion (boundary layer diffusion), intra-particle diffusion (internal diffusion) and binding of Cr(VI) to the available sites (adsorption reaction). In the current study, four reaction models and two diffusion models were used to investigate the adsorption mechanism.

Adsorption Reaction Models

Kinetic parameters for pseudo 1st order, pseudo 2nd order, Ritchie's second order and Pseudo-nth order are given in Table 5 and 6. Error functions for these models are presented in SI in Table S5 and S6. In the case of pseudo first-order (PFO) model,[38] for BC1 value of q_e (0.293–8.12 mg g^{-1}) increases with increasing initial concentration (1–100 mg L^{-1}), as shown in Table 5. As seen from the results of the error functions, a low correlation coefficient (R^2 = 0.976–0.995) and high error functions (ERRSQ = 0.0005–2.5; HYBRID = 2.88–8.09) indicate a modest fitting of this model on BC1. The BC2 value of q_e (0.333-9.49 mg g^{-1}) increased with increasing initial concentration (1–100 mg L^{-1}), as shown in Table 6. As seen from the results of the error functions, a low correlation coefficient (R^2 = 0.981–0.987) and high error functions (ERRSQ = 0.0002–2.3; HYBRID = 1.5–5.03) indicate the modest fitting of this model. Therefore, the results suggest that the pseudo first-order (PFO) kinetic adsorption model is not applicable in the current study.

In the case of pseudo 2_{nd}-order (PSO) model,[38] for the BC1 value of q_e (0.293–8.12 mg g^{-1}) increases with increasing initial concentration (1–100 mg L^{-1}), as expected, as shown in Table 5, but the difference between q_{exp} and q_e from the model varies from 1.36–3.41 %. The BC2 value of q_e (0.333–9.493 34 mg g^{-1}) increases with increasing initial concentration (1–100 mg L^{-1}), as expected, as shown in Table 6, but the difference between q_{exp} and q_e from the model varies from 0.166–2.908 %. Tables 5 & 6 show that as the initial concentration of Cr(VI) increased, the initial rate of sorption (h_2) values increased from 0.011 to 0.435 mg g^{-1} min^{-1} (BC1) and 0.101 to 0.655 mg g^{-1} min^{-1} (BC2) due to the greater driving force at higher initial concentrations. Moreover, with increasing initial concentration, the time required for reaching a specific fractional uptake increased, and subsequently, the K_2 rate constants decreased from 0.124–0.006 min^{-1} (BC1) and 0.904–0.007 min^{-1} (BC2). As seen from the results of the error functions, high correlation coefficients R^2 = 0.9999–0.9995 and R^2 = 0.9991–0.9998 exist for BC1 and BC2. In addition, other error functions are given in SI, such as ERRSQ and HYBRID,

Table 4. Isotherm models for Cr(VI) adsorption on BC2.

Isotherm Models	Parameters	20 °C	25 °C	30 °C	35 °C
Langmuir	q_m (mg g^{-1})	24.261	21.501	19.000	11.547
	K_L (L mg^{-1})	0.007	0.010	0.015	0.034
	R_L	0.993–0.586	0.99–0.504	0.985–0.395	0.967–0.225
	R^2	0.998	0.997	0.997	0.998
Freundlich	K_F (mg g^{-1}) / (mg L^{-1})^n	0.293	0.407	0.570	1.021
	n	1.281	1.379	1.476	1.957
	R^2	0.999	0.999	0.992	0.995
BET	Q_S (mg g^{-1})	23.21	14.933	20.793	14.236
	C_{BET} (L mg^{-1})	67.231	121.690	92.898	201.107
	C_S	9093.815	9093.000	9093.422	9092.918
	R^2	0.999777	0.996395	0.995618	0.988921

for both BC1 and BC2 are very low, which indicates that the PSO kinetic adsorption model is suitable for biochar in the current study. Additionally, based on the study of error functions of isotherm and kinetic experiments, it can be concluded that ERRSQ is the best criterion for optimizing relevant isotherm and kinetic models.

The physical meaning of Ritchie's equation[16] is that adsorption is dominated by adsorption in active sites. For BC1, the value of q_{inf} increases with increasing initial concentration, as expected (0.302–8.34 mg g^{-1}), and the difference between q_{exp} and q_{inf} from the model varies between 1.35–3.3 %. (Table 5) The rate constant α increases nonlinearly with increasing concentration (0.037–0.052 min^{-1}). Analysis of error functions shows that RSO gives a modest fitting for the current kinetic study that is slightly better than PSO. For BC2 the value of q_{inf} increases with increasing initial concentration, as expected (0.334–9.69 mg g^{-1}), and the difference between q_{exp} and q_{inf} from the model varies between –0.16–2.8 %.(Table 6). The rate constant α decreases nonlinearly with increasing concentration (0.3–0.05 min^{-1}). Analysis of error functions shows that RSO gives a modest fitting for the current kinetic study that is slightly better than PSO.

The PNO model[17] mainly represents the adsorption processes such that the order factor is between 1 and 2 or larger than 2. For BC1, the value of q_e increases with increasing initial concentration, as expected (0.30–8.35 mg g^{-1}), and the difference between q_{exp} and q_e from the model varies between 0.7–3.9 % (Table 5). The order of equation n remains close to 2, varying from 1.83 to 2.3. The rate constant K_n decreased nonlinearly (0.11–0.006 $(min^{-1})(mg\ g^{-1})^{(1-n)}$) with increasing concentration. For BC2, the value of qe increases with increasing initial concentration, as expected (0.33–9.6 mg g^{-1}), and the difference between q_{exp} and q_e from the model varies between –0.15–2.5 % (Table 6). The order of equation n remains close to 2, varying from 1.88 to 2.1. The rate constant K_n decreased nonlinearly (0.11–0.006 $(min^{-1})(mg\ g^{-1})^{(1-n)}$) with increasing concentration. A close value of n to 2 in both cases indicates that PSO is more applicable in the current study than PFO. Additionally, the decreasing value of K_n shows that adsorption slows down with increasing concentration. Analysis of error functions

Table 5. Kinetic models for Cr(VI) adsorption on BC1.

C_{ini} / mg L^{-1}	1	5	10	20	50	100
$q_{exp.}$ / mg g^{-1}	0.293	0.892	1.352	2.395	4.960	8.120
Pseudo–first order						
q_{cal} / mg g^{-1}	0.253	0.857	1.298	2.29	4.763	7.8
K_1 / min^{-1}	3.245×10^{-2}	3.788×10^{-2}	2.771×10^{-2}	4.175×10^{-2}	3.242×10^{-2}	3.32×10^{-2}
q_e / %	–13.528	–3.95	–3.964	–4.394	–3.988	–3.944
R^2	0.994809	0.987506	0.989184	0.976126	0.985193	0.984812
Pseudo–second order						
q_{cal} / mg g^{-1}	0.302	0.912	1.398	2.427	5.094	8.336
K_2 / g mg^{-1} min^{-1}	1.236×10^{-1}	6.721×10^{-2}	3.018×10^{-2}	2.854×10^{-2}	1.02×10^{-2}	6.264×10^{-3}
h /mg $g^{-1}min^{-1}$	1.129×10^{-2}	5.587×10^{-2}	5.899×10^{-2}	1.682×10^{-1}	2.601×10^{-1}	4.353×10^{-1}
Qe / %	3.321421	2.160673	3.411815	1.364432	2.687661	2.658791
R^2	0.999641	0.999471	0.999980	0.998782	0.999995	0.999985
Ritchie's second order equation						
α / min^{-1}	0.037	0.061	0.042	0.069	0.051	0.052
q_{inf} / mg g^{-1}	0.302	0.912	1.398	2.427	5.094	8.336
q_e / %	3.215102	2.115130	3.299041	1.346112	2.617247	2.589951
R^2	0.999641	0.999471	0.999980	0.998782	0.999995	0.999985
Pseudo–n^{th} order						
q_{cal} / mg g^{-1}	0.300	0.899	1.402	2.492	5.091	8.349
N	1.939	1.830	2.026	2.305	1.994	2.016
K_n / min^{-1} / $(mg\ g^{-1})^{(1-n)}$	0.114	0.063	0.030	0.033	0.011	0.006
Q_e / %	2.576028	0.704700	3.557014	3.917954	2.561080	2.739917
R^2	0.999666	0.999700	0.999983	0.999411	0.999995	0.999986

Table 6. Kinetic models for Cr(VI) adsorption on BC2.

C_{ini} / mg L^{-1}	1	5	10	20	50	100
$q_{exp.}$ / mg g^{-1}	0.333	0.892	1.460	2.620	5.560	9.493
Pseudo–first order						
q_{cal} / mg g^{-1}	0.324	0.860	1.399	2.525	5.362	9.154
K_1 / min^{-1}	1.705×10^{-1}	1.369×10^{-1}	6.356×10^{-2}	4.533×10^{-2}	3.342×10^{-2}	4.022×10^{-2}
q_e / %	–2.419805	–3.679869	–4.153062	–3.627677	–3.551982	–3.568904
R^2	0.986632	0.981031	0.987183	0.984667	0.985934	0.987354
Pseudo–second order						
q_{cal} / mg g^{-1}	0.334	0.891	1.465	2.663	5.721	9.693
K_2 / g mg^{-1} min^{-1}	9.039×10^{-1}	6.721×10^{-2}	7.853×10^{-2}	2.943×10^{-2}	9.357×10^{-3}	6.967×10^{-3}
h /mg $g^{-1}min^{-1}$	1.010×10^{-1}	5.587×10^{-2}	1.685×10^{-1}	2.087×10^{-1}	3.063×10^{-1}	6.546×10^{-1}
Qe / %	0.546565	–0.165547	0.323049	1.636385	2.907996	2.109665
R^2	0.999811	0.999121	0.999564	0.999601	0.999801	0.999487
Ritchie's second order equation						
α / min^{-1}	0.302	0.235	0.115	0.078	0.054	0.068
q_{inf} / mg g^{-1}	0.334	0.891	1.465	2.663	5.721	9.693
q_e / %	0.578722	–0.165770	0.321933	1.609790	2.824736	2.065996
R^2	0.999810	0.999121	0.999564	0.999601	0.999801	0.999487
Pseudo–n^{th} order						
q_{cal} / mg g^{-1}	0.333	0.891	1.476	2.656	5.702	9.597
N	1.917	2.003	2.108	1.967	1.963	1.876
K_n / min^{-1} / $(mg\ g^{-1})^{(1-n)}$	0.790	0.265	0.079	0.031	0.010	0.009
Q_e / %	0.202743	–0.147989	1.052267	1.358611	2.499455	1.087967
R^2	0.999899	0.999123	0.999676	0.999593	0.999814	0.999628

shows that PNO gives the best fit for kinetic data with error values better than other kinetic models. Based on error functions (Tables 5 & 6), kinetic data fitting in terms of best to least is as follows: PNO > RSO > PSO > PFO.

Adsorption Internal Diffusion Models

Internal diffusion models assume that the diffusion of adsorbate within the adsorbent is the slowest step. The diffusion of adsorbate in the liquid film around the adsorbent and the adsorption onto the active sites are instantaneous. Boyd's internal diffusion model and Weber-Morris internal diffusion model were used to investigate the adsorption mechanism in the current study. Conventionally, the adsorption of heavy metals on char occurs through four different mechanisms.[39,40] The first is the transport of the adsorbate (in this case, heavy metals such as chromium) from the bulk solution to the boundary layer of the BC (bulk diffusion). The second is the migration of the adsorbate through the boundary layer. Third, intraparticle diffusion occurs by the migration of the adsorbate from the surface toward the available active sites on the adsorbent within the internal surface of the BC (pore). Finally, the adsorption of heavy metals occurs on the entire surface through the active sites of BC.

Boyd's model[19] was proposed by Kumar et al. (2014) to predict the actual slowest step in the adsorption process and by Viegas et al. (2014) for estimating intraparticle diffusion coefficients in adsorption processes. The difference in estimated value of q_e from q_{exp} in Boyd's internal diffusion model is 2.7–4.7 % (BC1) and 3.6–5 % (BC2). The value of B was estimated using nonlinear analysis as 0.013–0.022 min^{-1} (BC1) and 0.019–0.08 min^{-1} (BC2). Parameters for this model given in table 7 and 8 while error functions for Boyd's internal diffusion model given in SI table S7 and S8) show that this model is applicable to the current study. The diffusion coefficients were also calculated using equation 13, as given in table 2 in SI. The D_i in this study varied from 7.3 to 12.7×10^{-4} cm^2 min^{-1} (BC1) and 1.1 to 4.6×10^{-3} cm^2 min^{-1} (BC2)according to this model. The D_i for BC2 according to this model is 1.04 to 6.2 times higher than that for BC1.

Table 7. Kinetic parameters for Cr(VI) adsorption onto BC1 with Boyd's internal diffusion model.

C_{ini} / mg L^{-1}	1	5	10	20	50	100
$Q_{cal.}$ / mg g^{-1}	0.280	0.861	1.282	2.279	4.711	7.718
B / min^{-1}	0.013	0.020	0.015	0.022	0.018	0.018
D / mm	1.5	1.5	1.5	1.5	1.5	1.5
D_i / mm^2 s^{-1}	1.22078×10^{-5}	1.90319×10^{-5}	1.43605×10^{-5}	2.11413×10^{-5}	1.69429×10^{-5}	1.72416×10^{-5}
q_e / %	–4.295076	–3.566370	–5.181112	–4.856212	–5.028086	–4.947566
R^2	0.948241	0.944101	0.952983	0.945522	0.952986	0.952736

Table 8. Kinetic parameters for Cr(VI) adsorption onto BC2 with Boyd's internal diffusion model.

C_{ini} / mg L^{-1}	1	5	10	20	50	100
$Q_{cal.}$ / mg g^{-1}	0.323	0.868	1.392	2.503	5.303	9.058
B / min^{-1}	0.080	0.060	0.035	0.026	0.019	0.023
D / mm	1.5	1.5	1.5	1.5	1.5	1.5
D_i / mm^2 s^{-1}	7.57475×10^{-5}	5.65688×10^{-5}	3.34059×10^{-5}	2.42931×10^{-5}	1.76296×10^{-5}	2.17292×10^{-5}
q_e / %	–2.764861	–2.691296	–4.667970	–4.450282	–4.612687	–4.582802
R^2	0.182713	0.505113	1.079133	1.981412	4.692037	7.474876

Table 9. Kinetic parameters for Cr(VI) adsorption onto BC1 with the Weber-Morris Intra-particle diffusion model (IPD).

C_{ini} / mg L^{-1}	1	5	10	20	50	100
Stage I						
k_{ip} / mg g^{-1} min$^{-1/2}$	0.028	0.106	0.139	0.296	0.550	0.909
C_{ip} / mg g^{-1}	0	0	0	0	0	0
D / mm	1.5	1.5	1.5	1.5	1.5	1.5
D_i / mm^2 min^{-1}	7.425×10^{-3}	1.105×10^{-2}	8.320×10^{-3}	1.196×10^{-2}	9.672×10^{-3}	9.845×10^{-3}
Time / min	0–40	0–40	0–40	0–40	0–40	0–40
R^2	0.992642	0.989924	0.992703	0.982094	0.992609	0.992844
Stage II						
k_{ip} / mg g^{-1} min$^{-1/2}$	0.012	0.026	0.052	0.072	0.168	0.270
C_{ip} / mg g^{-1}	0.115	0.529	0.607	1.369	2.562	4.268
D / mm	1.5	1.5	1.5	1.5	1.5	1.5
D_i / mm^2 min^{-1}	1.386×10^{-3}	5.977×10^{-3}	2.457×10^{-2}	4.752×10^{-2}	2.594×10^{-1}	6.699×10^{-1}
Time / min	40–120	40–120	40–120	40–120	40–120	40–120
R^2	0.997211	0.989756	0.988149	0.985811	0.986980	0.989270
Stage III						
k_{ip} / mg g^{-1} min$^{-1/2}$	1.839×10^{-3}	3.760×10^{-3}	8.208×10^{-3}	1.107×10^{-2}	2.563×10^{-2}	4.262×10^{-2}
C_{ip} / mg g^{-1}	0.244	0.794	1.146	2.116	4.310	7.047
D / mm	1.5	1.5	1.5	1.5	1.5	1.5
D_i / mm^2 min^{-1}	3.106×10^{-5}	1.298×10^{-4}	6.187×10^{-4}	1.125×10^{-3}	6.034×10^{-3}	1.668×10^{-2}
Time / min	120–720	120–720	120–720	120–720	120–720	120–720
R^2	0.960196	0.935244	0.923286	0.896542	0.929579	0.914105

Table 10. Kinetic parameters for Cr(VI) adsorption onto BC2 with the Weber-Morris Intra-particle diffusion model (IPD).

C_{ini} / mg L^{-1}	1	5	10	20	50	100
Stage I						
k_{ip} / mg g^{-1} min$^{-1/2}$	0.056	0.145	0.207	0.334	0.628	1.152
C_{ip} / mg g^{-1}	0	0	0	0	0	0
D / mm	1.5	1.5	1.5	1.5	1.5	1.5
D_i / mm^2 min^{-1}	0.023	0.149	0.304	0.793	2.798	9.434
Time / min	0–40	0–40	0–40	0–40	0–40	0–40
R^2	0.918437	0.930759	0.976458	0.986480	0.992244	0.990280
Stage II						
k_{ip} / mg g^{-1} min$^{-1/2}$	0.002	0.057	0.107	0.068	0.209	0.877
C_{ip} / mg g^{-1}	0.300	0.706	0.992	1.688	2.747	6.128
D / mm	1.5	1.5	1.5	1.5	1.5	1.5
D_i / mm^2 min^{-1}	3.664×10^{-5}	2.328×10^{-2}	8.194×10^{-2}	3.283×10^{-2}	0.309	5.465
Time / min	40–120	40–120	40–120	40–120	40–120	40–120
R^2	0.805852	0.854960	0.927803	0.993177	0.953196	0.984587
Stage III						
k_{ip} / mg g^{-1} min$^{-1/2}$	2.913×10^{-4}	4.779×10^{-5}	5.024×10^{-3}	7.499×10^{-3}	2.512×10^{-2}	3.270×10^{-2}
C_{ip} / mg g^{-1}	0.325	0.882	1.329	2.418	4.927	8.631
D / mm	1.5	1.5	1.5	1.5	1.5	1.5
D_i / mm^2 min^{-1}	6.028×10^{-7}	1.623×10^{-8}	1.794×10^{-4}	3.996×10^{-4}	4.484×10^{-3}	7.600×10^{-3}
Time / min	120–720	120–720	120–720	120–720	120–720	120–720
R^2	0.915360	0.898403	0.968921	0.888510	0.921328	0.882448

Due to the possibility of mass transport through the diffusion mechanism as the rate controlling step, the adsorption mechanism was also explored by the Webber-Morris intraparticle diffusion model. The linear plot for some parts does not pass through the origin, which suggests that adsorption proceeds via a complex mechanism consisting of both surface adsorption and the intra-particle transport within the pores of the adsorbent. Table 9 and 10 contain kinetic parameters for Cr(VI) adsorption onto BC1 and BC2 with Weber-Morris Intra-particle diffusion model (IPD) respectively. The corresponding error functions are provided in supplementary information as Tables S9 and S10. The plot represents mainly three regions or stages of adsorption. The first region (0–40 min) represented the external surface adsorption (i.e., film diffusion), where adsorption is instantaneous with k_{ip} = 0.028–0.909 mg g^{-1} min$^{-1/2}$ for BC1 and k_{ip} = 0.056–1.152 mg g^{-1} min$^{-1/2}$ for BC2. Here, the value of the boundary layer thickness C_{ip} is zero, which shows that the process is diffusion controlled. The diffusion coefficient D_i values increase gradually from 7.4×10^{-3}–11.96×10^{-3} mm^2 min^{-1}, for BC1 and 0.0226–9.434 mm^2 min^{-1} for BC2 which shows that the process has started. D_i values for BC2 are much larger than BC1 which shows much faster kinetics. However, this increase is erratic; hence, in stage 1, the correlation between K_{id} and C_{ini} is not significant. The second region (40–120 min) is related to intraparticle diffusion, where adsorption is gradual with k_{ip} = 0.012–0.27 mg g^{-1} min$^{-1/2}$ in case of BC1 and k_{ip} = 0.0023–0.877 mg g^{-1} min$^{-1/2}$ in case of BC2. approximately 2.3 to 4.15 times (BC1) and 24 to 1.3 times (BC2) smaller than at stage I. Large value of boundary layer thickness C_{ip} = 0.12–4.27 mg g^{-1} for BC1 and C_{ip} = 0.3–6.13 mg g^{-1} for BC2 shows that film diffusion and intraparticle diffusion both play a role in controlling adsorption. In this stage, Cr(VI) gradually occupied the surface sites of biochar and slowly transferred to the inner parts of the adsorbent. The diffusion coefficient Di values increase significantly from 1.38×10^{-3}–0.67 mm^2 min^{-1} for BC1 and 3.66×10^{-5}–5.47 mm^2 min^{-1} for BC2. This is approximately 0.2 to 68 times for BC1 which shows fast process kinetics. However, in case of BC2 there is a decrease of about 1.7 to 616 times in D_i in stage I, which shows slower process kinetics. There is a strong correlation between K_{id} and C_{ini} here in both BC1 and BC2. The third region (120–720 min), or a portion nearly parallel to the *x*-

axis, indicates equilibrium adsorption.[42] This third region is related to the large boundary layer thickness, where adsorption is very low, with k_{pi} = 1.8 × 10^{-3}–42.6 × 10^{-3} mg g^{-1} $min^{-1/2}$ for BC1 and k_{pi} = 4.8 × 10^{-5}–32.7 × 10^{-3} mg g^{-1} $min^{-1/2}$ much smaller than at stage II. Highest value of boundary layer thickness C_{ip} = 0.24–7.05 mg g^{-1} for BC1and C_{ip} = 0.3–8.63 mg g^{-1} for BC2 shows that the boundary layer has practically stopped the adsorption. Here, all available pores of the adsorbent were taken up by Cr(VI), external mass transfer declined dramatically, and the process actually stopped due to no film or intraparticle diffusion. Hence, equilibrium adsorption occurs, where the D_i values are at a minimum level for BC1 (3.11 × 10^{-5}–16.68 × 10^{-3} mm^2 min^{-1}) and BC2 (1.62 × 10^{-8}–7.6 × 10^{-3} mm^2 min^{-1}) which shows that the process ceases. Reviewing the error functions for all stages, it is clear that the Weber Morris IPD model can be used for modelling the process under study.

The plot thus suggests that the adsorption process proceeds via surface adsorption and intraparticle or pore diffusion. From these three regions, the rate limiting step can be estimated. Thus, the ratio of time taken for film diffusion to the time taken for intra-particle diffusion was estimated (Table 9). If the ratio is more than unity (i.e., > 1), it reveals that film diffusion is the dominant step in the process. However, if the ratio is less than unity (i.e., < 1), it indicates that the adsorption process is controlled by intraparticle diffusion. Here, since the ratio is 0.5, adsorption seems to be controlled by intraparticle diffusion.

The value of Di from Weber Morris is 2 to 647 times larger than that from Boyd's internal diffusion model. Comparing the error functions, it is clear that the overall Weber Morris intraparticle diffusion model is more applicable than Boyd's internal diffusion model.

Thermodynamic of Cr(VI) Adsorption on Biochar

The positive value of ΔH confirmed that Cr(VI) adsorption on biochar is endothermic,[17] hence, the increase in temperature favors the adsorption process. The endothermic nature is also verified from our earlier results showing an increase in the sorption/removal capacity (Q_{max}) with increasing temperature (Table 3). Furthermore, the value of ΔH ranges between 2.1 and 20.9 kJ mol^{-1} and between 20.9 and 418.4 kJ mol^{-1} in the case of physisorption and chemisorption, respectively.[43] For BC1 Δ*H* is 74.483 kJ mol^{-1} and BC2 59.51 kJ mol^{-1}, which indicates chemisorption in the current study. A positive ΔS of 0.337 kJ mol^{-1} K^{-1} (BC1) and 0.285 kJ mol^{-1} K^{-1} (BC2) is attributed to the increase in randomness at the solid–liquid interface.[18] A negative Δ*G* suggested that the adsorption process was spontaneous in the studied temperature range (Table 11). An increase in negative Δ*G* with an increase in temperature indicates greater adsorption at higher temperatures.[18] Based on thermodynamic isotherms and kinetic studies, the adsorption of Cr(VI) on both BC1 and BC2 exhibits characteristics of both monolayer and multilayer adsorption on a heterogeneous surface.

Table 11. Thermodynamics parameters of Cr (VI) adsorption on BC1 & BC2.

Biochar	Temperature	*K*	Δ*G* / kJ mol^{-1}	Δ*H* / kJ mol^{-1}	Δ*S* / kJ mol^{-1} K^{-1}
BC1	20 °C	20444.979	–24.192	74.483	0.337
	25 °C	37447.853	–26.105		
	30 °C	62306.800	–27.826		
	35 °C	99275.15	–29.478		
BC2	20 °C	20344.774	–24.180	59.508	0.285
	25 °C	28424.968	–25.422		
	30 °C	44181.346	–26.96		
	35 °C	64866.162	–28.388		

CONCLUSION

Beechwood chip biochar (BC1) and garden green waste biochar (BC2) effectively remove Cr(VI) from aqueous solutions, with maximum adsorption capacities of 8.13 and 9.49 mg g^{-1}, respectively, at ideal pH of 5.0. While these capacities are adequate for low to moderate chromium contamination, additional optimization is required for heavily polluted waterways. The adsorption process was spontaneous, heterogeneous, and chemisorptive. The equilibrium data fit well to both Langmuir and Freundlich models (R^2 = 0.999) and had low error values. Kinetics research revealed that the adsorption process adhered to the pseudo-second order (PSO) model, with intra-particle diffusion (Weber-Morris model) playing an important role in rate regulation. Among error functions, ERRSQ was the most trustworthy criterion for model optimization. The thermodynamic values supported the spontaneous and endothermic nature of Cr(VI) adsorption on biochars. The comparatively moderate adsorption capacities reflect the influence of the biochars' physical and chemical features, such as surface area, porosity, and functional groups, and are consistent with previous research. Future study should focus on evaluating biochars in real contaminated water matrices, comparing different biochars with diverse properties, and investigating further changes to optimize adsorption performance for practical applications.

Acknowledgment. This research did not receive any support or specific grant from funding agencies in the public, commercial, or not-for-profit sectors.

Supplementary Information. Supporting information to the paper is attached to the electronic version of the article at: http://doi.org/10.5562/cca4096.

PDF files with attached documents are best viewed with Adobe Acrobat Reader which is free and can be downloaded from Adobe's web site.

REFERENCES

[1] E. Brasili, I. Bavasso, V. Petruccelli, G. Vilardi, A. Valletta, C. Dal Bosco, A. Gentili, G. Pasqua, L. Di Palma, *Sci. Rep.* **2020**, *10*, 1920. https://doi.org/10.1038/s41598-020-58639-7

[2] G. Choppala, N. Bolan, B. Seshadri, *J. Hazard. Mater.* **2013**, *261*, 718–724. https://doi.org/10.1016/j.jhazmat.2013.03.040

[3] Y. P. Zhang, V. S. K. Adi, H. L. Huang, H. P. Lin, Z. H. Huang, *J. Ind. Eng. Chem.* **2019**, *76*, 240–244. https://doi.org/10.1016/j.jiec.2019.03.046

[4] B. Thangagiri, A. Sakthivel, K. Jeyasubramanian, S. Seenivasan, J. D. Raja, K. Yun, *Chemosphere* **2022**, *286*, 131598. https://doi.org/10.1016/j.chemosphere.2021.131598

[5] S. M. Shaheen, N. K. Niazi, N. E. Hassan, I. Bibi, H. Wang, D. C. Tsang, Y. S. Ok, N. Bolan, J. Rinklebe, *Int. Mater. Rev.* **2019**, *64*, 216–247. https://doi.org/10.1080/09506608.2018.1473096

[6] X. Xu, H. Huang, Y. Zhang, Z. Xu, X. Cao, *Environ. Pollut.* **2019**, *244*, 423–430. https://doi.org/10.1016/j.envpol.2018.10.068

[7] A. D. Igalavithana, S. Mandal, N. K. Niazi, M. Vithanage, S. J. Parikh, F. N. Mukome, M. Rizwan, P. Oleszczuk, M. Al-Wabel, N. Bolan, *Crit. Rev. Environ. Sci. Technol.* **2017**, *47*, 2275–233. https://doi.org/10.1080/10643389.2017.1421844

[8] J. Wan, F. Liu, G. Wang, W. Liang, C. Peng, W. Zhang, K. Lin, J. Yang, *Bioresour. Technol.* **2021**, *337*, 12538. https://doi.org/10.1016/j.biortech.2021.125382

[9] S. Kloss, F. Zehetner, B. Wimmer, J. Buecker, F. Rempt, G. Soja, *J. Plant Nutr. Soil Sci.* **2014**, *177*, 3–15. https://doi.org/10.1002/jpln.201200282

[10] Y. Ding, Y. Liu, S. Liu, Z. Li, X. Tan, X. Huang, G. Zeng, Y. Zhou, B. Zheng, X. Cai, *RSC Adv.* **2016**, *5223*, 523. https://doi.org/10.1039/C5RA26248H

[11] I. Langmuir, *J. Am. Chem. Soc.* **1918**, *40*, 1361–1403. https://doi.org/10.1021/ja02242a004

[12] H. M. F. Freundlich, *J. Phys. Chem.* **1906**, *57*, 385–471.

[13] S. Brunauer, P. H. Emmett, E. Teller, *J. Am. Chem. Soc.* **1938**, *60*, 309–319. https://doi.org/10.1021/ja01269a023

[14] S. Lagergren, *Kungl. Svenska Vetenskapsakademiens, Handlingar* **1898**, *24*, 1–39.

[15] G. Blanchard, M. Maunaye, G. Martin, *Water Res.* **1984**, *18*, 1501–1507. https://doi.org/10.1016/0043-1354(84)90124-6

[16] A. G. Ritchie, *J. Chem. Soc. Faraday Trans.* **1977**, *173*, 1650–1653. https://doi.org/10.1039/f19777301650

[17] A. Ozer, *J. Hazard. Mater.* **2007**, *141*, 753–761. https://doi.org/10.1016/j.jhazmat.2006.07.040

[18] W. J. Weber, J. C. Morris, *J. Sanitary Eng. Div.* **1963**, *89*, 31–39. https://doi.org/10.1061/JSEDAI.0000430

[19] G. E. Boyd, J. Schubert, A. W. Adamson, *J. Am. Chem. Soc.* **1947**, *69*, 2818–282. https://doi.org/10.1021/ja01203a064

[20] X. Zhou, X. Zhou, *Chem. Eng. Commun.* **2014**, *201*, 1459–1467. https://doi.org/10.1080/00986445.2013.818541

[21] S. Rehman, A. Adil, A. J. Shaikh, J. A. Shah, M. Arshad, M. A. Ali, M. Bilal, *Environ. Sci. Pollut. Res.* **2018**, *25*, 31579–31592. https://doi.org/10.1007/s11356-018-2958-2

[22] R. R. Karri, J. N. Sahu, N. S. Jayakumar, *J. Taiwan Inst. Chem. Eng.* **2017**, *80*, 472–487. https://doi.org/10.1016/j.jtice.2017.08.004

[23] A. L. Prasad, T. Santhi, S. Manonmani, *Arabian J. Chem.* **2015**, *8*, 343–35. https://doi.org/10.1016/j.arabjc.2011.01.020

[24] L. T. Popoola, *Heliyon* **2019**, *5*, e01153. https://doi.org/10.1016/j.heliyon.2019.e01153

[25] S. M. Miraboutalebi, et al., *Process Saf. Environ. Prot.* **2017**, *106*, 191–202. https://doi.org/10.1016/j.psep.2017.01.010

[26] K. V. Kumar, K. Porkodi, F. Rocha, *J. Hazard. Mater.* **2008**, *150*, 158–165. https://doi.org/10.1016/j.jhazmat.2007.09.020

[27] T. M. Abdel-Fattah, M. E. Mahmoud, S. B. Ahmed, M. D. Huff, J. W. Lee, S. Kumar, *J. Ind. Eng. Chem.* **2015**, *22*, 103–109. https://doi.org/10.1016/j.jiec.2014.06.030

[28] C. Li, L. Zhang, Y. Gao, A. Li, *Waste Manag.* **2018**, *79*, 625–637. https://doi.org/10.1016/j.wasman.2018.08.035

[29] S. Zhu, X. Huang, D. Wang, L. Wang, F. Ma, *Chemosphere* **2018**, *207*, 50–59. https://doi.org/10.1016/j.chemosphere.2018.05.046

[30] Y. Qiu, Q. Zhang, B. Gao, M. Li, Z. Fan, W. Sang, H. Hao, X. Wei, *Environ. Pollut.* **2020**, *265*, 11501. https://doi.org/10.1016/j.envpol.2020.115018

[31] R. Coşkun, C. Soykan, M. Saçak, *Sep. Purif. Technol.* **2006**, *49*, 107–11. https://doi.org/10.1016/j.seppur.2005.09.002

[32] Y. Shi, R. Shan, L. Lu, H. Yuan, H. Jiang, Y. Zhang, Y. Chen, *J. Clean. Prod.* **2020**, *254*, 119935. https://doi.org/10.1016/j.jclepro.2019.119935

[33] J. Zhang, S. Chen, H. Zhang, X. Wang, *Bioresour. Technol.* **2017**, *238*, 484–49. https://doi.org/10.1016/j.biortech.2017.04.081

[34] T. W. Weber, R. K. Chakravorti, *AIChE J.* **1974**, *20*, 228–238. https://doi.org/10.1002/aic.690200204
[35] F. Haghseresht, G. Q. Lu, *Energy Fuels* **1998**, *12*, 1100–1107. https://doi.org/10.1021/ef9801165
[36] S. Nakajima, S. Araki, R. Sasamoto, Y. Kanda, S. Yamanaka, *Chemosphere* **2022**, *287*, 132257. https://doi.org/10.1016/j.chemosphere.2021.132257
[37] H. A. Murad, M. Ahmad, J. Bundschuh, Y. Hashimoto, M. Zhang, B. Sarkar, Y. S. Ok, *Environ. Res.* **2022**, *204*, 112125. https://doi.org/10.1016/j.envres.2021.112125
[38] J. Wang, X. Guo, *J. Hazard. Mater.* **2020**, *122156*. https://doi.org/10.1016/j.jhazmat.2020.122156
[39] H. Shang, Y. Li, J. Liu, Y. Wan, Y. Feng, Y. Yu, *Bioresour. Technol.* **2020**, *314*, 123708. https://doi.org/10.1016/j.biortech.2020.123708
[40] W. J. Weber, R. K. Chakravorti, *J. Environ. Eng.* **1984**, *110*, 899–917. https://doi.org/10.1061/(ASCE)0733-9372(1984)110:5(899)
[41] R. M. C. Viegas, M. Campinas, H. Costa, M. J. Rosa, *Adsorption* **2014**, *20*, 737–74. https://doi.org/10.1007/s10450-014-9617-9
[42] C. R. Girish, V. R. Murty, *Int. J. Chem. Eng.* **2016**, *5809505*. https://doi.org/10.1155/2016/5809505
[43] R. E. Treybal, *Mass Transfer Operations*. Vol. 1 (New York : McGraw-Hill, ©**1980**., 1981)
[44] S. Sikarwar, R. Jain, *Water Air Soil Pollut*. **2014**, *225*, 1842. https://doi.org/10.1007/s11270-013-1842-4